Ocean Sci., 21, 643–659, 2025
https://doi.org/10.5194/os-21-643-2025

Ocean Science Open Access EGU

The influence of a submarine canyon on the wind-driven downwelling circulation over the continental shelf

Pedro A. Figueroa[1], **Gonzalo S. Saldías**[1,2], **and Susan E. Allen**[3]

[1]Departamento de Física, Facultad de Ciencias, Universidad del Bío-Bío, Concepción, Chile
[2]Centro de Investigación Oceanográfica COPAS Coastal, Universidad de Concepción, Concepción, Chile
[3]Department of Earth, Ocean and Atmospheric Sciences, University of British Columbia, Vancouver, Canada

Correspondence: Gonzalo S. Saldías (gsaldias@ubiobio.cl)

Received: 28 July 2024 – Discussion started: 2 August 2024
Revised: 4 November 2024 – Accepted: 15 January 2025 – Published: 14 March 2025

Abstract. The response of a coastal ocean model, simulating a typical eastern boundary system, to downwelling-favorable winds with and without the presence of a submarine canyon is studied. Three contrasting bathymetric configurations, considering shelves with different depths and slopes, are evaluated. Experiments without a submarine canyon represent the well-known downwelling circulation and cross-shore structure with a downwelling front and the development of frontal instabilities generating density anomalies in the bottom layer. The presence of the submarine canyon drives important changes in cross-shore flows, with opposing velocities on either side of the canyon. Onshore (offshore) and downward (upward) velocities develop in the upstream (downstream) side of the canyon in the time-dependent and advective phases. Instabilities develop and are modified principally downstream of the canyon. Overall, the net impact of the canyon is to enhance offshore and downward transport. However, particle tracking experiments reveal that particles can become trapped inside the canyon in an anticyclonic circulation when the particles pass the canyon over the continental slope or when particles inside the canyon are affected by downwelling conditions. Overall, $\sim 20\,\%$–$23\,\%$ ($\sim 15\,\%$–$18\,\%$) of particles released directly upstream (in the canyon) at depths below the continental shelf become trapped inside the canyon until the end of the simulations (15 d).

1 Introduction

Submarine canyons are common features along continental shelves, acting as pathways for water exchange between the continental slope and the coastal ocean through upwelling and downwelling dynamics, facilitating the cross-shore exchanges of heat, nutrients, and organic matter. These cross-shore exchanges are tied to the circulation induced by the canyon as it breaks the along-isobath flow, generating ageostrophic circulation and enhanced cross-shore transport (Allen and Durrieu de Madron, 2009; Saldías and Allen, 2020). The effects of submarine canyons on circulation have been studied with in situ observations (e.g., Hickey, 1997; Allen et al., 2001; Flexas et al., 2008; Sobarzo et al., 2016; Brun et al., 2023), modeling approaches (e.g., Klinck, 1996; She and Klinck, 2000; Jordi et al., 2005; Spurgin and Allen, 2014; Ahumada-Sempoal et al., 2015; Saldías and Allen, 2020), and theoretical scaling analysis (Allen and Hickey, 2010; Howatt and Allen, 2013). Modeling efforts have shown that the circulation around a submarine canyon depends primarily on the direction of the incident flow, generating different circulation patterns in the presence of right- or left-bounded flows. For upwelling-favorable flow (left-/right-bounded in the Northern/Southern Hemisphere), the canyon enhances the upwelling (Kämpf, 2007), driving a pool of dense water on the shelf downstream of the canyon (Saldías and Allen, 2020). In contrast, downwelling-favorable flow (right-/left-bounded in the Northern/Southern Hemisphere) promotes an antisymmetrical circulation, with onshore and downward velocities along the upstream side and offshore/upward velocities in the downstream side of the

canyon (Klinck, 1996; Spurgin and Allen, 2014). The patterns of circulations are further modified by the stratification in the canyon, with contrasting patterns related to the Burger number (Spurgin and Allen, 2014), and the orientation of the canyon relative to the incident flow (Ahumada-Sempoal et al., 2015; Wang et al., 2022).

Regardless of the importance of submarine canyons as conducts of cross-shore transport between the deep and coastal oceans and their related ecological characteristics, these sites are still poorly sampled and studied. Observational studies are difficult due to the complex topography and the common presence of fisheries (which lead to the loss of instruments), which enhances the importance of theoretical and modeling approaches. These modeling studies have given insights into the circulation around these sites in idealized (e.g., Klinck, 1996; She and Klinck, 2000; Kämpf, 2006, 2007, 2009, 2012; Spurgin and Allen, 2014; Zhang and Lentz, 2017; Kämpf, 2018, 2019; Saldías and Allen, 2020) and realistic conditions (Jordi et al., 2005; Connolly and Hickey, 2014; Ahumada-Sempoal et al., 2015; Wang et al., 2022). However, these studies have been primarily focused on upwelling conditions around submarine canyons (e.g., Klinck, 1996; Kämpf, 2006; Howatt and Allen, 2013; Connolly and Hickey, 2014; Saldías and Allen, 2020), and downwelling conditions have been significantly less studied. The few modeling studies that have addressed the downwelling response have presented two types of circulation, controlled by the Burger number at the canyon (Spurgin and Allen, 2014). Furthermore, the idealized studies have used a body-force forcing condition (Klinck, 1996; She and Klinck, 2000) or a combination of body force and local wind forcing (Spurgin and Allen, 2014), while the realistic setups have resolved downwelling conditions by means of downwelling currents (Jordi et al., 2005; Ahumada-Sempoal et al., 2015). In the case of downwelling wind-driven experiments, the influence of a shelf valley, shallower than a submarine canyon, has been studied (Zhang and Lentz, 2017), as well as the impact of a submarine canyon using only surface wind forcing (Spurgin and Allen, 2014). However, the response of the flow field to deep and steep submarine canyons forced only by local downwelling winds and with different continental slopes, typical of eastern boundary systems, has not been addressed yet in detail. In downwelling-favorable wind conditions, a downwelling front is formed near the bottom, with isopycnals tilted downwards (Lentz and Fewings, 2012; Kämpf, 2019). This front develops baroclinic instabilities (Feliks and Ghil, 1993; Brink, 2016, 2024) and can generate an active eddy field in some regions. How this downwelling front and the frontal instabilities interact near/around a submarine canyon has not been addressed yet.

The upwelling and downwelling effects of a submarine canyon in the local circulation are different, with a stronger response for upwelling-favorable conditions than for its downwelling counterpart (Klinck, 1996; Zhang and Lentz, 2017). However, high-productivity and biological hotspots have been observed and predicted in downwelling submarine canyons (Skliris and Djenidi, 2006; Flexas et al., 2008; Mordy et al., 2019), even when the net effect of submarine canyons in downwelling conditions is to enhance the downwelling response (Klinck, 1996; She and Klinck, 2000). These biological characteristics have been hypothesized to be linked to local onshore and positive vertical velocities in downwelling canyons, as well as the effects of the cyclonic and anticyclonic circulations that could induce the trapping of particles (Skliris and Djenidi, 2006; Spurgin and Allen, 2014). In a realistic simulation in Blanes Canyon in the NW Mediterranean Sea, Ahumada-Sempoal et al. (2015) found that particles tend to aggregate in the head of the canyon by the presence of a seasonally varying downwelling current. Furthermore, submarine canyons could be connected through particle transport in a regional context in downwelling conditions, which could be important for pelagic larval stages (Clavel-Henry et al., 2019). However, this trapping of particles has not been studied for wind-driven downwelling events, such as those developed in eastern boundary systems by synoptic storm events. This is an important feature considering that submarine canyons have also been associated with biological hotspots and enhanced productivity compared to the adjacent slopes (e.g., Allen et al., 2001; Skliris and Djenidi, 2006; De Leo et al., 2010; Ceramicola et al., 2015; Santora et al., 2018). The present study aims to further understand the induced effects of a submarine canyon in the context of wind-driven downwelling forcing; how these effects are observed in the local circulation, cross-shore transport, and vertical transport; and the trapping and onshore transport of particles in the coastal ocean. A high-resolution numerical model, forced with constant downwelling-favorable winds and variable bathymetric configurations, is used with and without a submarine canyon. These simulations are also analyzed in a Lagrangian particle tracking experiment to study the effects of the canyon on particles along the shelf. Section 2 presents the details of the model configurations and particle experiments, Sect. 3 describes the main results, Sect. 4 gives a detailed discussion of our findings, and the conclusions are given in Sect. 5.

2 Methodology

2.1 Model configuration and experiments

We used the Regional Ocean Modeling System (ROMS) (Shchepetkin and McWilliams, 2005), a primitive-equation model that uses finite differences to resolve the hydrostatic primitive equations. Vertical differencing is achieved with terrain-following (sigma) coordinates (Song and Haidvogel, 1994). The model is run with a third-order upstream horizontal and a fourth-order centered vertical advection scheme for momentum and tracers to avoid spurious vertical velocities at the canyon rim due to stratified flow over steep to-

pography using sigma coordinates (Dawe and Allen, 2010). The horizontal pressure gradient is treated with a spline density Jacobian (Shchepetkin and McWilliams, 2003). Vertical mixing was computed using the Mellor–Yamada level 2.5 closure scheme (Mellor and Yamada, 1982), and the background vertical viscosity and diffusivity were set to 1×10^{-5} and $5 \times 10^{-6}\,\mathrm{m^2\,s^{-1}}$, respectively. Bottom stress is calculated with a quadratic drag law using a bottom roughness of 2×10^{-2} m, as done by previous studies in banks and canyons using ROMS (Whitney and Allen, 2009; Li et al., 2021).

The experiments consisted of an idealized coastal ocean, typical of an eastern boundary system, with dimensions of 155 km in the cross-shore direction and 600 km in the alongshore direction, with higher resolution near the coast that diminishes offshore. The grid spacing is 0.5 km in both cross-shore and alongshore directions in the region around the canyon (Fig. 1b). From 50 km offshore the grid resolution decreases towards the western boundary with a maximum grid spacing of 10 km. Three types of bathymetric configurations, already described by Saldías and Allen (2020), were used by changing the shelf slope. The maximum depth was 500 m offshore in all configurations. Deep-shelf experiments were based on the bathymetry used by Klinck (1996) and derived works, where a canyon is defined as

$$H(x,y) = H_\mathrm{m} - \frac{H_\mathrm{s}}{2}\left[1 - \tanh\frac{-x - x_\mathrm{o}(y)}{a}\right], \tag{1}$$

where H_m is the maximum depth of the domain (500 m), H_s is the depth change from the continental shelf to the open ocean (400 m), a is the transition scale defining the slope of the cross-shelf profile (5 km), and $x_\mathrm{o}(y)$ is the location of the shelf break, defined as

$$x_\mathrm{o}(y) = x_\mathrm{n} + x_\mathrm{b}\left[1 - \exp\frac{-\left(y^2 - y_\mathrm{o}^2\right)}{2b^2}\right], \tag{2}$$

where x_n is the nominal distance of the head of the canyon from the coastal wall (12 km), x_b is the distance added to x_n to reach the shelf break (10 km), y_o is the location of the center of the canyon (at $y = 0$ km), and b is the width scale of the canyon (2.5 km). This configuration produces a canyon that is 10 km wide in its mouth and 20 km long from its mouth to its head and with a sidewall steepness of ~ 0.065. Intermediate and shallow experiments were run with more realistic sloping shelves by changing some key parameters in Eqs. (1) and (2), as in Saldías and Allen (2020). The experiments were configured with 30 s coordinate levels, using an increased resolution near the surface and bottom to resolve the boundary layers, with $\theta_\mathrm{s} = 3$ and $\theta_\mathrm{b} = 1$, Vstretching = 4, Vtransform = 2, and hcline = 50 m following Shchepetkin and McWilliams (2009). The domain has three open boundaries (north, south, and offshore), which are better suited for canyon experiments (e.g., Dinniman and Klinck, 2002; Zhang and Yankovsky, 2016; Zhang and Lentz, 2017) where implicit gravity wave radiation conditions (Chapman, 1985) and the Flather radiation scheme (Flather, 1976) were applied to the surface elevation and depth-averaged horizontal velocities, respectively. Orlanski radiation conditions (Orlanski, 1976) were applied to the baroclinic velocities, temperature, and salinity on the western boundary. A local two-dimensional model of the northern and southern boundaries was run to extract the local fields for those boundary conditions (e.g., Gan and Allen, 2005; Castelao and Barth, 2006; Saldías and Allen, 2020).

The six experiments (three bathymetries, canyon cases, and no-canyon cases) were forced with only a horizontally uniform northward (downwelling-favorable) surface wind stress that is ramped up from 0 to $0.03\,\mathrm{N\,m^{-2}}$ in 5 d (from days 10 to 15) and then maintained constant for the following 10 d of the simulations. The model was run free during the first 10 d to let transients decay. Initial conditions in temperature and salinity are the same as those used by Saldías and Allen (2020) based on the average stratification conditions off Oregon (see Fig. 1c).

Dimensionless numbers are calculated for each experiment and summarized together with bathymetric constant and wind forcing in Table 1. The vertical aspect ratio H_s/L is calculated defining H_s as the depth of the canyon from the shelf to the bottom of the canyon, and L is the length of the canyon, defined using the shallowest isobath related to the canyon rim. A description of the incoming velocity interacting with the canyon is given by the Rossby number (Ro):

$$Ro = \frac{U}{fL}, \tag{3}$$

where U is the incoming velocity interacting with the canyon or shelf (i.e., upstream of the canyon location), calculated by averaging the meridional velocity over the continental shelf; f is the Coriolis parameter; and L is the length of the canyon or shelf width. Another version of the Rossby number but using the radius of curvature R rather than the length of the canyon is also calculated (Ro_c) following Howatt and Allen (2013). In addition, a description of the stratification conditions is given by the Burger number Bu:

$$Bu = \frac{N H_\mathrm{sb}}{fL}, \tag{4}$$

where N is the mean buoyancy frequency over the upstream continental shelf, H_sb is the depth of the shelf, and f and L are the same as for the Rossby number. A complementary version of Bu, called the topographic Burger number, is calculated as follows:

$$S = s\frac{N}{f}, \tag{5}$$

where s is the continental shelf slope, calculated by taking the slope between the depth at the beginning of the shelf break and the coast.

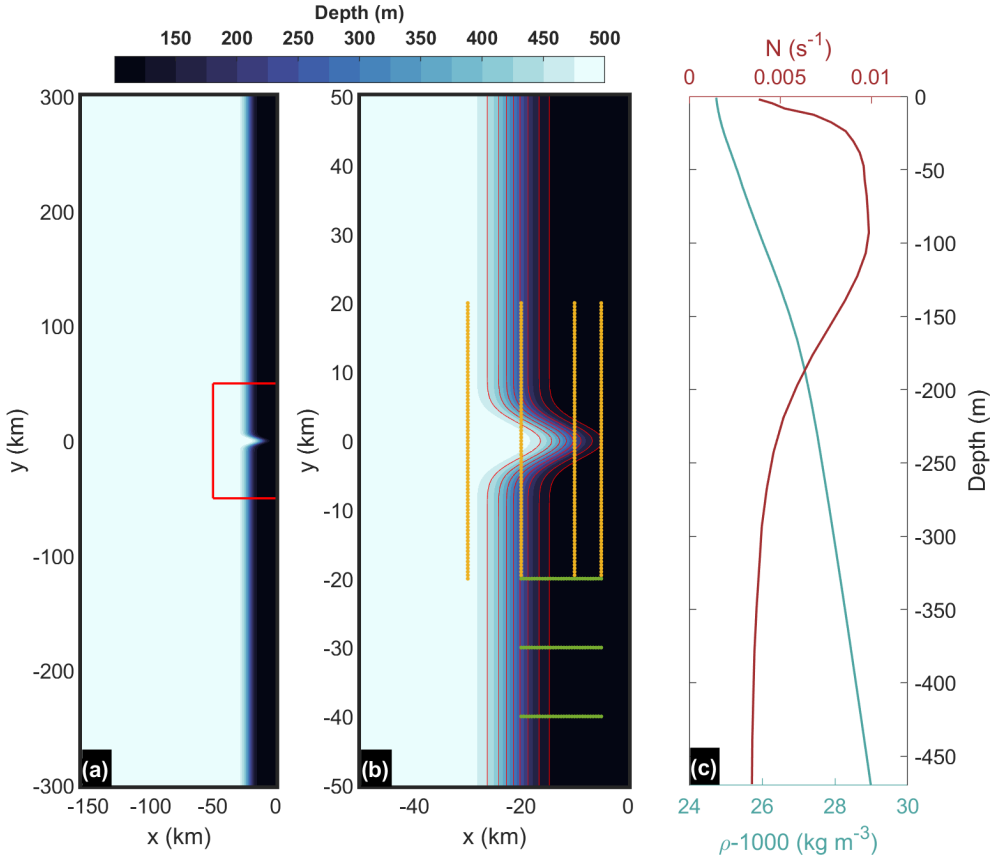

Figure 1. **(a)** Model domain bathymetry (colors; m) with the location of the submarine canyon enclosed in a red box. **(b)** Zoomed-in view of the area of the submarine canyon enclosed in **(a)**, with the 100, 125, 150, 200, 250, 300, 350, 400, and 450 m isobaths shown in the red contours. The yellow and green lines indicate the vertical planes where particles were released for particle tracking experiments. **(c)** Initial conditions in density (green line) and stratification (buoyancy frequency, red line) imposed for the whole domain shown in **(a)**.

Table 1. List of experiments with and without a submarine canyon under contrasting bathymetric configurations. H_s/L is the vertical aspect ratio (depth of the shelf break over the length of the canyon). Ro and Ro_c are the Rossby numbers using the length of the canyon/shelf and the radius of the curvature, respectively.

Exp	Exp1	Exp2	Exp3	Exp4	Exp5	Exp6
Canyon	No	Yes	No	Yes	No	Yes
Shelf	Deep shelf	Deep shelf	Intermediate shelf	Intermediate shelf	Shallow shelf	Shallow shelf
$\lvert\tau_y\rvert$ (N m^{-2})	0.03	0.03	0.03	0.03	0.03	0.03
H_m (m)	500	500	500	500	500	500
H_s (m)	400	400	446	446	486.5	486.5
x_n ($\times 10^3$ m)	12	12	12	12	12	12
x_b ($\times 10^3$ m)	10	10	10	10	10	10
a ($\times 10^3$ m)	5	5	10	10	10	10
b ($\times 10^3$ m)	2.5	2.5	2.5	2.5	2.5	2.5
H_s/L	–	0.01	–	0.009	–	0.005
Ro	0.143	0.187	0.178	0.196	0.198	0.165
Ro_c	–	0.4	–	0.43	–	0.37
Bu	–	1.323	–	0.774	–	0.222
S	0	0	0.126	0.143	0	0.07

2.2 Particle experiments

Horizontal and vertical velocity fields from the ROMS experiments were used as inputs for offline particle tracking experiments using the Parcels (Probably A Really Computationally Efficient Lagrangian Simulator) v2 code (Delandmeter and van Sebille, 2019). These Lagrangian experiments were run to assess the effects of canyon-driven circulation on the transport of particles in the canyon and along the continental shelf. Parcels is a Python-based particle tracking module that allows for the release of passive and active particles using outputs of ocean circulation models. We defined three areas of release based on the main characteristics of the canyon-induced circulation: (1) three zonal planes upstream of the canyon ($y = -20$ km, $y = -30$ km, and $y = -40$ km) reaching from near the coast to the rim of each canyon configuration ($-30\,\text{km} < x < -5\,\text{km}$) and from the surface to the maximum depth of the continental shelf and (2) meridional planes at $x = -30$ km, $x = -20$ km, $x = -10$ km, and $x = -5$ km, extending in the meridional direction from $y = -20$ km to $y = 20$ km and from the surface down to the bottom, with a maximum depth of 500 m in $x = -30$ km. (3) Lastly, particles were released inside the canyon at different horizontal planes, starting at the rim depth and reaching down to the bottom of the canyon for each bathymetric configuration. These planes extend from $x = -5$ km to $x = -20$ km and $y = -10$ km to $y = 10$ km in the horizontal. The particles were configured using a fourth-order Runge–Kutta advection scheme that allows vertical displacement. The particles were defined as non-buoyant elements and without diffusivity. They were released at day 10 of each simulation and were tracked until the end of the simulations (day 25). Velocity fields from ROMS were interpolated at each time step to z levels from 5 to 400 m with a 2.5 m resolution and then used as input to the Parcels environment. Particles that were trapped by the seafloor or stopped by the topography were discarded from our analysis, and thus we only maintain particles that presented displacement through the entire period of tracking.

3 Results

3.1 Downwelling patterns: canyon vs. no-canyon experiments

Variations in downwelling patterns are influenced by slope configuration and the presence of a submarine canyon (Fig. 2). In deep-shelf experiments lacking a canyon, downward depth-averaged velocities occur near the coast, attributed to water descent from downwelling winds (Fig. 2a), and horizontal velocities are predominantly northward. In the case of intermediate- and shallow-shelf experiments (Fig. 2b and c), instabilities emerge farther offshore, with intensified vertical velocities along the coast at the location of the downwelling front.

The presence of a submarine canyon induces notable changes in its vicinity (Fig. 2d–f), where upstream and downstream areas are defined as being south and north of the canyon axis ($y = 0$ km), respectively. In the deep-shelf experiments, downward velocities occur around the upstream side of the canyon, while upward velocities prevail on the downstream wall. These vertical velocities extend up to 15 km offshore in a cross-shore band and exhibit a near-symmetrical distribution. A slight cyclonic deflection in horizontal velocities is observed over the canyon. Frontal instabilities persist in the intermediate- and shallow-shelf experiments, with intensified vertical velocities near the canyon (Fig. 2e and f). In the intermediate-shelf experiment, interactions of these instabilities with the canyon alter the canyon-induced dipole of vertical velocities seen in the deep-shelf experiment, generating pronounced vertical motions from the coast up to 8 km offshore (Fig. 2e). In the shallow-shelf experiment, a stronger dipole of vertical velocities, compared to the other experiments, is evident from the coast to approximately 10 km offshore, with depth-averaged vertical velocities being stronger than in the deep-shelf experiment.

The cross-shore structure of downwelling circulation exhibits variations with changes in bathymetry (Fig. 3). In the deep-shelf experiments (Fig. 3, left column panels), surface and bottom Ekman layers are discernible in cross-shore velocities, featuring onshore transport at the surface and offshore transport at the bottom of the shelf. Isopycnals tilt downwards, with the formation of a downwelling front near the coast by day 25. Northward flow prevails across the domain, characterized by two primary jets in the cross-shore direction. One lies over the shelf break at around 100 m below the surface, whereas a second, stronger jet develops next to the coast and extends through most of the water column. As bathymetry becomes shallow in the intermediate and shallow experiments, instabilities modify the cross-shore downwelling structure and the position of the northward jet (Fig. 3, central and right columns). The downwelling front is located around $x = -5$ km and $x = -10$ km (denoted by the isopycnal 25.2 kg m^{-3}) in the intermediate- and shallow-shelf experiments, respectively, coinciding with the bending of isopycnals towards the bottom. These positions align with regions of strong vertical velocities (Fig. 2), indicating that instabilities do not form in deep-shelf experiments by day 25 due to incomplete development of the downwelling front. Regarding northward flow, relative zones of strong velocities are observed around the downwelling front in the intermediate-shelf case (around $x = -5$ km and $x = -10$ km), whereas the downwelling jet emerges just above the downwelling front at $x = -10$ km in shallow-shelf experiments (Fig. 2).

The influence of a submarine canyon induces notable alterations in cross-shore velocities (Fig. 4). Upstream, at $y = -15$ km, three layers of cross-shore velocities emerge

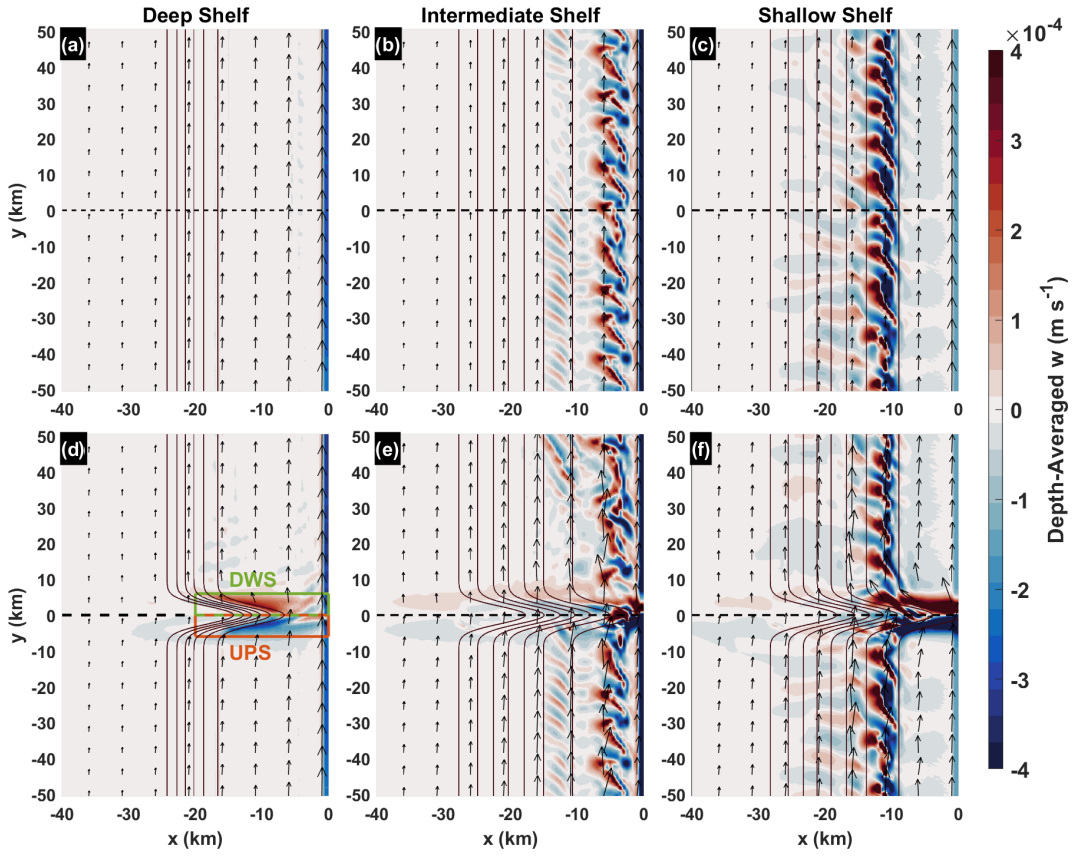

Figure 2. Depth-averaged vertical velocities (color) and depth-averaged horizontal currents (arrows) for **(a, c)** deep-, **(b, e)** intermediate-, and **(c, f)** shallow-shelf configurations with **(d–f)** and without **(a–c)** a submarine canyon at day 25.

in the deep-shelf experiment (Fig. 4m): the surface onshore Ekman layer, the bottom offshore Ekman layer, and an intermediate layer with weaker onshore velocities. This intermediate layer is consistent across all configurations, being modified by instabilities in the intermediate and shallow shelves. Alongshore velocities remain almost unchanged upstream of the canyon compared to the no-canyon counterparts in all bathymetric configurations. Along the canyon axis ($y = 0$ km), offshore and onshore velocities within the canyon tend to overcome the typical flow of Ekman layers (evident in the no-canyon cases in the deep-shelf experiments). Moreover, instabilities extend into the canyon in the intermediate and shallow experiments, inducing strong cross-shore exchanges. Isopycnals evolve from a tilted orientation within the canyon to nearly horizontal farther offshore. Alongshore velocities show a weak counter-current within the canyon compared to the prevalent northward flow in the intermediate- and shallow-shelf experiments. Downstream, at $y = 15$ km (Fig. 4a–f), a layer of offshore velocities extends from the base of the surface Ekman layer to the bottom. This layer is present in all cases, with some modifications near the coast due to instabilities in the intermediate- and shallow-shelf cases, suggesting that the canyon presence influences the circulation farther offshore. Notably, there are no significant changes in the cross-shore position of the downwelling jet after it passes the canyon (Fig. 3d–f vs. Fig. 4d–f).

The presence of a canyon is linked to an increase in the Rossby number in the deep and intermediate experiments but not in the shallow experiment, as short length scales are already present (Table 1). In general, flows in all six experiments are geostrophic. Regarding stratification, the presence of a canyon does not make a large difference. However, the stratification tends to diminish as the water column gets shallow over the continental shelf. This is evidenced by the Burger numbers with $Bu = 0$ and $S = 0$ in the shallow-shelf experiments, related to the density homogenization in the area selected to compute the numbers, caused by the faster evolution and displacement of isopycnals in this configuration compared to deep- and intermediate-shelf experiments.

Alongshore sections at two distinct locations ($x = -6$ km and $x = -13$ km) elucidate the canyon's impact on the vertical structure of the cross-shore velocities (Fig. 5). These locations were chosen based on the cores of higher variability observed in Fig. 2. In the absence of a canyon, the surface and bottom Ekman layers are clearly discernible in the deep-shelf experiment (Fig. 5a and g). However, the presence of

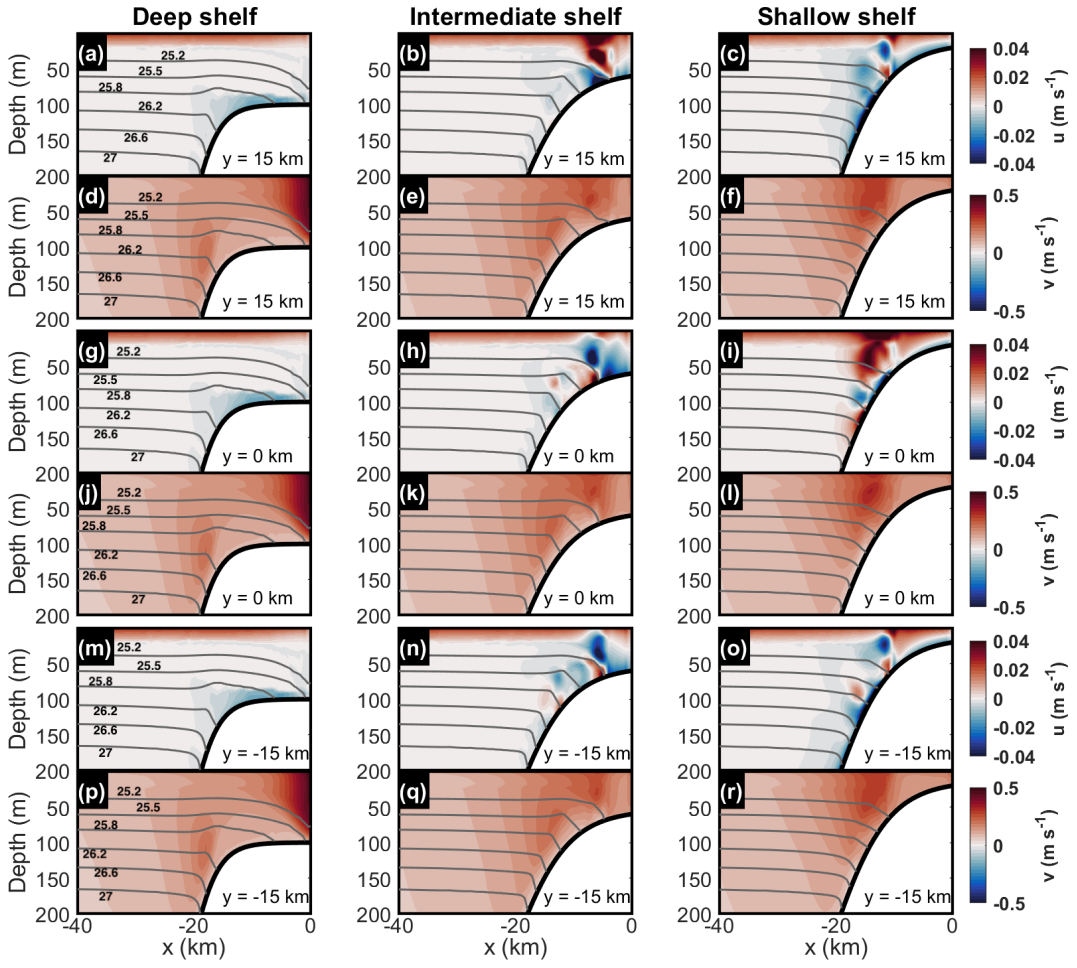

Figure 3. Cross-shore sections of velocity (color) and density (gray lines) fields at $y = 15$ km **(a–f)**, $y = 0$ km **(g–l)**, and $y = -15$ km **(m–r)** for the no-canyon simulations at day 25. The isopycnals shown for the deep-shelf case also correspond to the intermediate- and shallow-shelf cases.

a canyon induces a dipole of opposing cross-shore velocities over the canyon walls (Fig. 5d and j), disrupting the bottom Ekman layer over the canyon walls. At $x = -13$ km, cross-shore velocities are confined to the shelf near the canyon walls, without extending to the canyon bottom. Two weak counter-currents develop inside the canyon, generating contrasting circulation patterns. Offshore and onshore velocities induced by the canyon extend to the surface at this location, interacting with the surface Ekman layer. At $x = -6$ km, velocities extend throughout the entire canyon, with offshore velocities on the downstream side penetrating the base of the surface Ekman layer (Fig. 5j).

Cross-shore velocities primarily relate to instabilities in the intermediate experiments without a canyon (Fig. 5h). In the presence of a canyon, an anticyclonic circulation forms inside the canyon at $x = -13$ km, beneath a weak cyclonic dipole interacting with instabilities. Instabilities reappear approximately 30 km north of the canyon. At $x = -6$ km, instabilities dominate cross-shore velocities even in the presence of the canyon. Notably, there is a distinct modification of their structure as they pass over the canyon, with the patterns being different on the downstream side compared to the upstream side. In the shallow-shelf experiments, instabilities dominate the cross-shore velocity structure at $x = -13$ km. The presence of a canyon induces a cyclonic (anticyclonic) circulation over (inside) the canyon (Fig. 5f). Downstream, instabilities are minimally affected by the canyon. However, the nearshore cross-shore circulation ($x = -6$ km) mirrors that of the deep-shelf experiments, as instabilities are located farther offshore. The presence of a canyon disrupts bottom and surface Ekman layers, generating strong onshore (offshore) velocities upstream (downstream) of the canyon, affecting the entire water column (Fig. 5l).

The effects of the canyon are evident in the density variations observed between the canyon and no-canyon runs at the end of the simulations. In the deep-shelf experiments, a layer of lighter water is observed over the downstream shelf in the presence of the canyon (Fig. 6a), confined to the lower 20 m

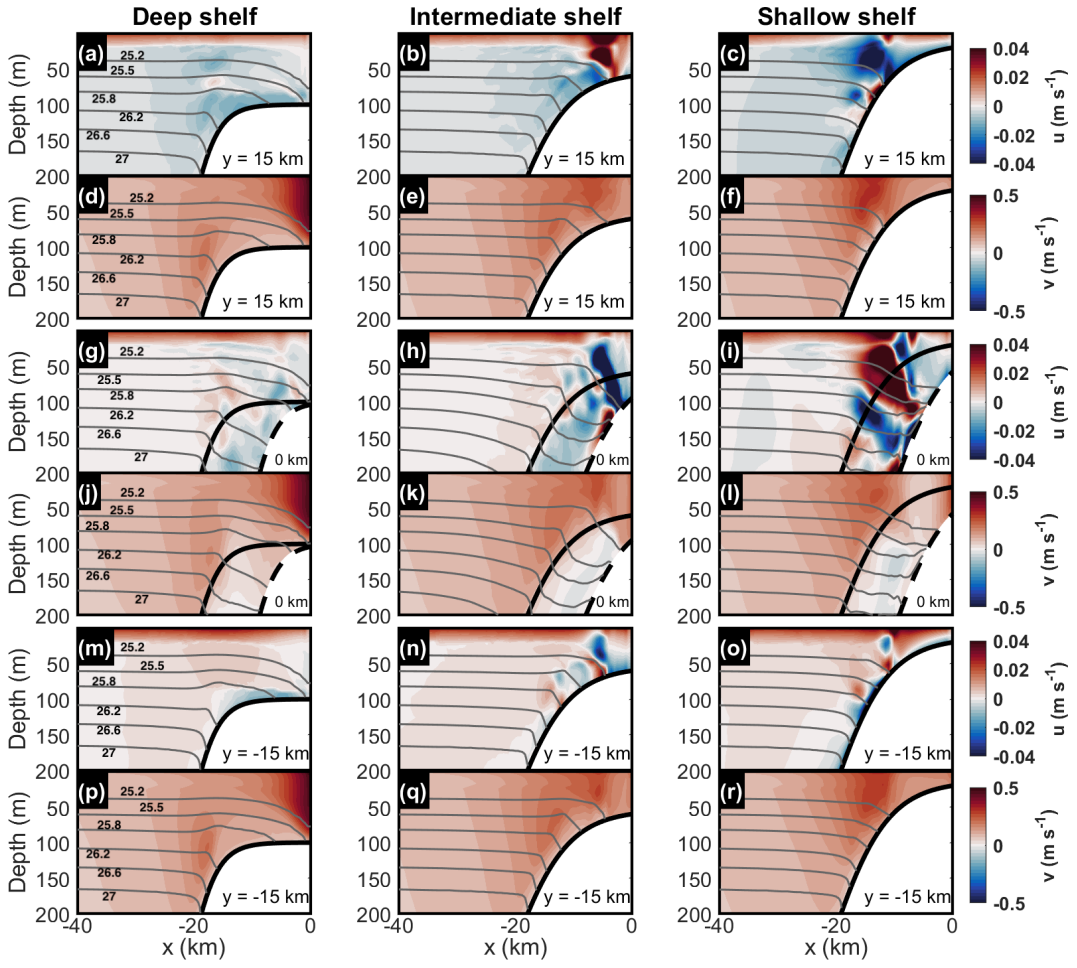

Figure 4. Cross-shore sections of velocity (color) and density (gray lines) fields at $y = 15$ km **(a–f)**, $y = 0$ km **(g–l)**, and $y = -15$ km **(m–r)** for the canyon simulations at day 25. The solid black lines denote the cross-shore bathymetry profile without the canyon ($y = 0$), whereas the dashed black lines indicate the bathymetry at the center of the canyon. The isopycnals shown for the deep-shelf case also correspond to the intermediate- and shallow-shelf cases.

and followed by a layer of higher-density water around 20–80 m from the surface, much clearer at $x = -13$ km (Fig. 6d and g). The difference in density near the coast is more pronounced, with faster advection of light surface water to the bottom in the presence of the canyon, resulting in lighter water compared to the no-canyon experiment at a given time. A column of negative anomalies also appears over the canyon axis due to the extended downward tilt of isopycnals in the canyon cases.

In the intermediate- and shallow-shelf experiments, the density differences clearly indicate modifications to the instabilities by the canyon. Upstream, there are no significant differences between the canyon and no-canyon experiments. However, after passing the canyon, positive and negative density anomalies are observed in both experiments, centered at $x = -6$ km in the intermediate configuration and at $x = -13$ km in the shallow configuration. These density differences align with the positions of the instabilities shown in Fig. 2 and only appear downstream, as upstream the instabilities have not yet interacted with the canyon. As these instabilities pass over the canyon, their wavelengths are altered, leading to local density anomalies compared to the distribution in the no-canyon scenarios. In the intermediate-shelf experiments, these instabilities affect up to 20 m below the surface near the coast, while in the shallow configuration, differences in density extend up to the surface at $x = -13$ km but are minimal near the coast.

3.2 Cross-shore and vertical transport

The spatial extent and magnitude of the cross-shore transport are significantly altered by the presence of a submarine canyon (Fig. 7). In the absence of a canyon, the primary cross-shore velocities consist of the Ekman layers during the advective phase, along with velocities induced by instabilities in the intermediate- and shallow-shelf experiments. Consequently, the deep-shelf experiment exhibits increasing

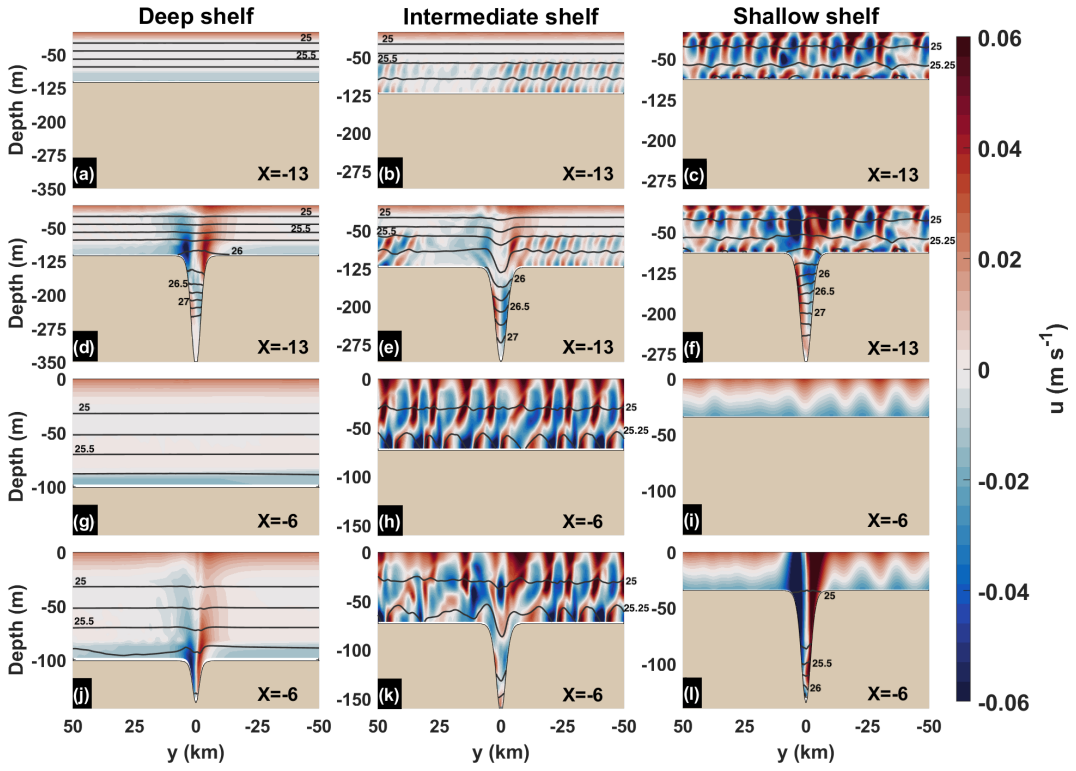

Figure 5. Alongshore sections of cross-shore velocity (color) and isopycnal (black lines, every 0.25 kg m^{-3}) fields at $x = -13$ km **(a–f)** and $x = -6$ km **(g–l)** comparing the no-canyon **(a–c; g–i)** and canyon **(d–f; j–l)** experiments at day 25.

onshore transport over the course of the simulation due to an imbalance between the surface and bottom Ekman layers (Fig. 7e), resulting in high cumulative onshore transport by the end of the simulation. In contrast, the intermediate- and shallow-shelf experiments evolve more rapidly, achieving a balance between the Ekman layers and having low cross-shore transport throughout the simulation.

In the case of the shallow shelf at $x = -13$ km, the presence of instabilities is evident in the variable cross-shore transport along the coast, resulting in fluctuating magnitudes, although with minimal impact on cumulative transport by the end of the period (Fig. 7b). The presence of the canyon induces a reduction in onshore transport in all three simulations (Fig. 7c and d). The temporal evolution shows an increase in offshore transport in all experiments in response to velocities generated around the canyon, transitioning to the advective phase where cross-shore transport becomes positive in the deep-shelf experiment and close to zero in the intermediate-shelf experiment. In contrast, the net transport remains negative in the shallow-shelf experiment, reflecting the influence of instabilities in the canyon experiment, but without reaching positive values and exhibiting a trend towards net offshore transport over the period. This trend is further highlighted in the cumulative transport in the canyon run, where the intermediate and shallow shelves consistently show consistent offshore transport, while the deep-shelf experiment exhibits net onshore transport from about day 21 onwards.

The spatial distribution of cross-shore transport underscores the significance of canyon-induced velocities (Fig. 7e and f). In the absence of a canyon, cross-shore transport remains relatively constant with minimal variations alongshore, attributed to the balance between Ekman layers. In the shallow case, where instabilities are fully developed at $x = -13$ km, high alongshore variability is observed. The presence of a canyon results in strong onshore transport upstream and offshore transport downstream of the canyon, with the greatest magnitudes observed in the deep-shelf experiment.

The vertical transport induced by the canyon at the shelf level (Fig. 8) exhibits an antisymmetrical response on the downstream and upstream sides of the canyon, consistent with the depth-averaged vertical velocities. By analyzing the net vertical transport into upstream (from $y = -6$ km to $y = 0$ km) and downstream (from $y = 6$ km to $y = 0$ km) components, it is evident that both sides of the canyon induce vertical transport of nearly equal magnitudes. Following day 20, fluctuations in vertical transport are observed in the intermediate- and shallow-shelf experiments, linked to the development and passage of instabilities near the canyon (Fig. 8c and e).

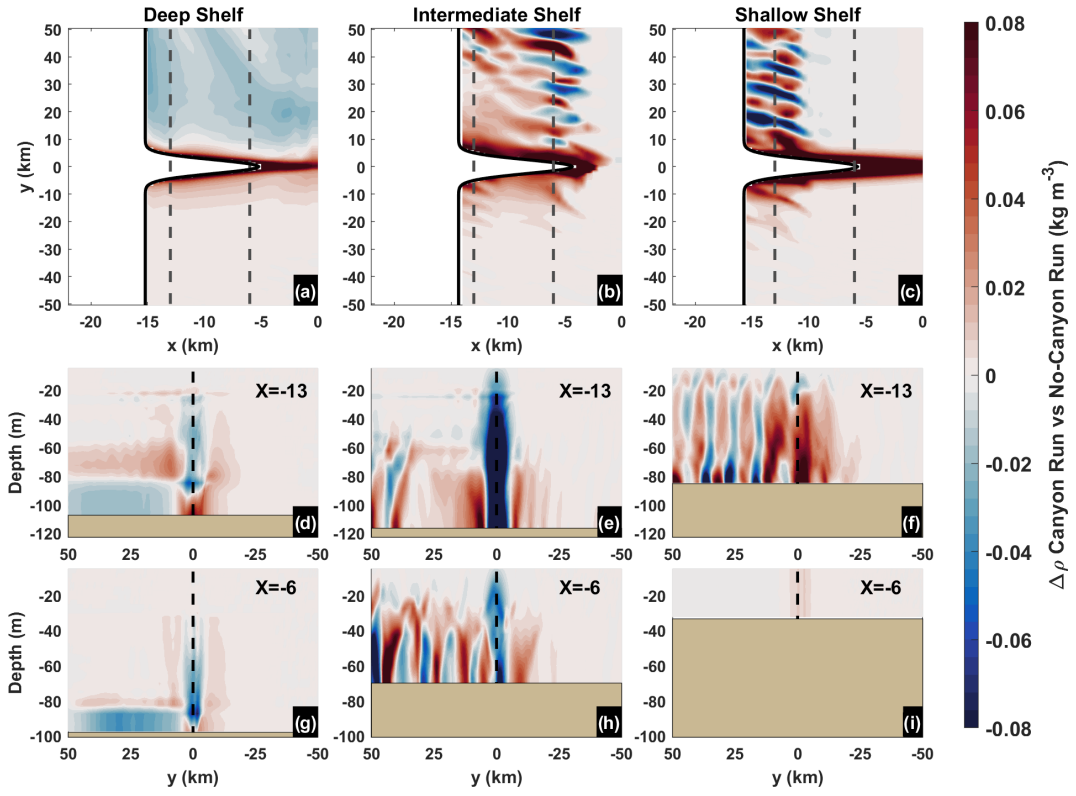

Figure 6. Density differences between the canyon runs (experiments 2, 4, 6) and no-canyon runs (experiments 1, 3, 5) at day 25. **(a–c)** Differences at the closest level to the bottom for each configuration. **(d–i)** Alongshore sections (gray lines in **a**–**c**) at $x = -13$ km and $x = -6$ km.

In all three simulations, a negative net transport, corresponding to negative velocities on both sides of the canyon, characterized the initial 5 d of the forcing period. Subsequently, a sign change occurs in the downstream side, while the upstream side maintains negative values, leading to a quasi-balance between upwelling and downwelling. The vertical transport stabilizes and remains relatively constant until the instabilities develop in the intermediate and shallow experiments. Notably, in the shallow-shelf case, vertical transport even approaches zero between days 16 and 20, indicating a balance between upwelling and downwelling (Fig. 8e). However, the overall effect of the submarine canyon results in a net downwelling throughout the simulation. The deep-shelf experiment exhibits greater vertical transport compared to the intermediate-shelf experiment (Fig. 8b and d).

3.3 Fate of particles under downwelling conditions

The velocity perturbations induced by the canyon result in significant cross-shore transport and vertical velocities around the canyon, contrasting with the experiments lacking a submarine canyon. An examination of particle dispersion along the shelf in the presence of a canyon reveals that particles can travel up to 15 km in the cross-shore direction along the canyon (Fig. 9). In contrast, the particles' cross-shore displacement reaches a maximum of 2 km outside the surface and bottom Ekman layer in experiments without a canyon (not shown), a trend consistent across all three bathymetric configurations.

For particles released upstream of the canyon (at $y = -20$ km), the presence of the canyon induces horizontal deflection in their trajectories throughout the water column (Fig. 9). This effect manifests as a cyclonic turn over the canyon following the isobaths, with particles returning to their original cross-shore positions after passing over the canyon, particularly for particles above the shelf. Conversely, particles at shelf-break depth (and below) tend to follow the isobaths and can become trapped within the canyon (Fig. 9a–c, yellow colors), exhibiting anticyclonic circulation patterns extending up to 15 km in length (Fig. 10a–c, yellow colors). The various slope configurations determine the depth at which particles may become trapped inside the canyon, as well as the quantity of particles entrapped. Steeper slopes tend to trap more particles than relatively flat shelves, with particles potentially remaining confined within the canyon for up to 15 d. Notably, particles released upstream at $y = -30$ km and $y = -40$ km did not show significant trapping within the canyon at any depth (not shown).

Particles released outside the canyon rim or over the shelf (yellow planes in Fig. 1) were influenced by the presence

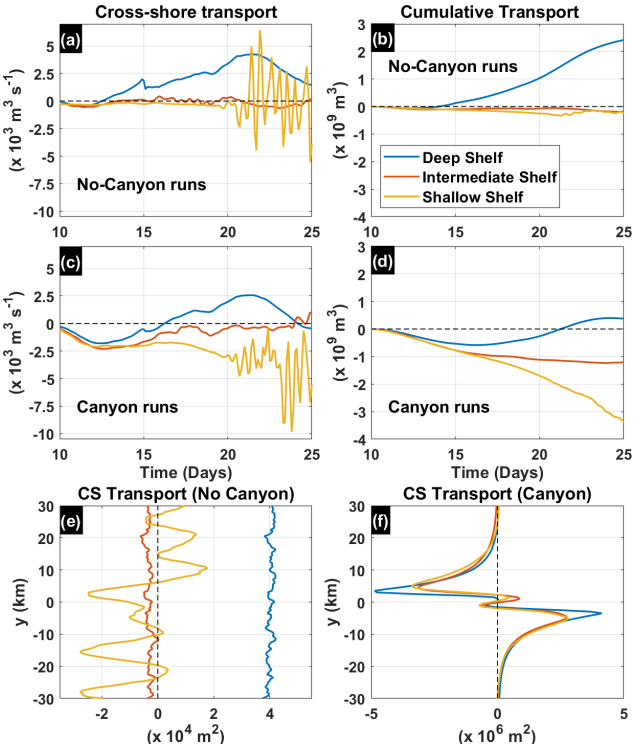

Figure 7. Cross-shore transport for all experiments at the plane farther from the coast shown in Figs. 6 and 7 ($x = -13$ km). **(a, b)** Cross-shore and cumulative transport for the no-canyon experiments. **(c, d)** Same as before but for the canyon experiments. **(e, f)** Alongshore distribution of the cross-shore transport for the no-canyon and canyon simulations integrated over the 25 d of the simulation. Note that the cross-shore transport is 2 orders of magnitude greater in the canyon simulations **(f)** than in its no-canyon counterpart **(e)**, and different scales are shown for a better description of the patterns in each case.

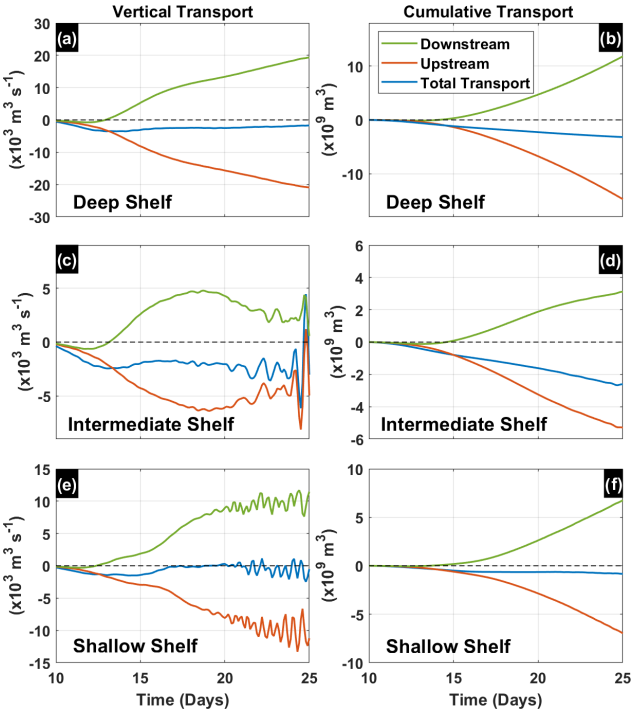

Figure 8. Vertical transport for the downstream and upstream areas in the three simulations with a submarine canyon, calculated at the depth of the shelf in the zonal extension between the coast and $x = -20$ km. **(a, c, e)** Vertical and **(b, d, f)** cumulative transport at **(a, b)** $z = -100$ m for the deep-shelf canyon, **(c, d)** $z = -60$ m for the intermediate-shelf canyon, and **(e, f)** $z = -20$ m for the shallow-shelf canyon. Every panel presents different scales in order to highlight the local vertical transport and its variability.

of the canyon (Fig. 9d–f), resulting in advection inside the canyon on the upstream side and subsequent advection outside the canyon on the downstream side. The particles were then carried northward by the geostrophic current, dispersing along the continental shelf. This effect is more pronounced with increasing depth and shelf slope, with particles following isobaths as they enter the canyon and traveling cross-shore up to 4 km, although they were not observed to become entrapped in any simulation.

Particles released at shelf-break depth, or within the canyon and parallel to the rim, either became trapped within the canyon with anticyclonic circulation or continued following isobaths before exiting at the canyon mouth, being advected northward by the current. Trapped particles within the canyon traveled up to 7 km onshore (Fig. 10), and only the particles released upstream of $y = -5$ km became trapped in the canyon. Overall, the vertical displacements were generally negative, with the vertical velocities induced by the submarine canyon (Fig. 2) not significantly affecting the vertical movements of the particles. Cross-shore velocities were identified as the primary pathway for trapping particles within the canyon.

Overall, around 20 % of particles become trapped up to the end of the experiments when they are released upstream (Fig. 9a–c) at $y = -20$ km at 115–185, 100–170, and 75–145 m for the deep-, intermediate-, and shallow-shelf experiments, respectively. The percentage of trapped particles appeared to increased with increasing slopes and decreasing shelf depths. Outside of the depth ranges shown in Fig. 9 (i.e., up to the surface and down to 400 m depth), the percentage of particle trapped diminished. In the case of the particles parallel to the coast at $x = -20$ km (Fig. 9d–f), between 15.5 %–18.5 % of particles released at 210–260, 200–250, and 190–240 m for the deep-, intermediate-, and shallow-shelf experiments, respectively, were trapped inside the canyon, with no clear pattern related to bathymetric changes.

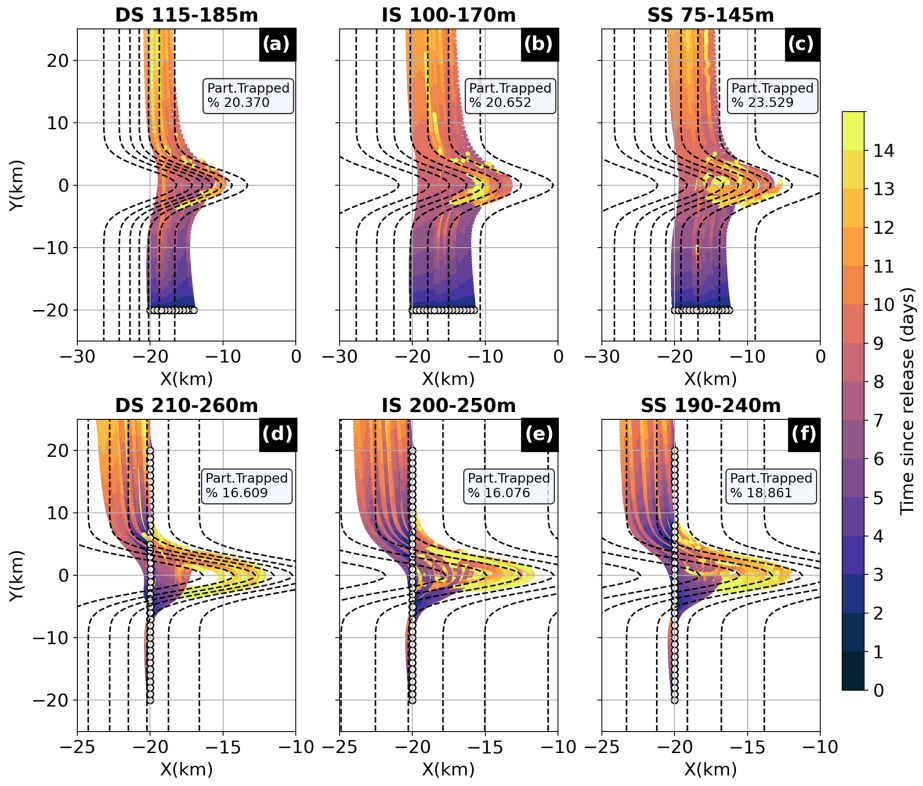

Figure 9. Examples of particle trajectories around a canyon for the three shelf configurations (deep shelf – DS, intermediate shelf – IS, shallow shelf – SS). The color indicates the time since the particles' release, whereas the white points denote their initial positions. Isobaths of the submarine canyon (from 100 to 400 m) are shown in dashed red lines. **(a–c)** Particle trajectories released in a zonal plane at $y = -20$ km. **(d–f)** Particle trajectories released in meridional planes at $x = -20$ km and $-20\,\text{km} \leq y \leq 20\,\text{km}$.

4 Discussion

Wind-driven downwelling is characterized by onshore Ekman transport, leading to an offshore pressure gradient force and poleward current, along with offshore transport in the bottom Ekman layer in eastern boundary systems (Austin and Lentz, 2002; Lentz and Fewings, 2012). Previous studies have demonstrated that the presence of a submarine canyon under downwelling-favorable conditions (by means of imposed currents) can amplify downwelling and alter local circulation (Klinck, 1996; She and Klinck, 2000; Skliris et al., 2001, 2002), resulting in onshore (offshore) and downward (upward) velocities on the upstream (downstream) side in both idealized (Klinck, 1996; Spurgin and Allen, 2014; Zhang and Lentz, 2017) and realistic simulations (Jordi et al., 2005; Ahumada-Sempoal et al., 2015). Our findings indicate a consistent presence of positive vertical velocities on the downstream side of the canyon, persisting almost continuously but subject to variations induced by passing instabilities over the canyon.

Moreover, notable onshore velocities are observed along the upstream side of the canyon, particularly around the rim. These canyon-induced velocities can induce local upwelling, even in regions experiencing downwelling-favorable wind conditions, facilitated by onshore upslope transport. However, the overall vertical transport around the canyon remains predominantly downward, with the upstream downward component slightly exceeding the downstream upward component. The net cross-shore transport demonstrates a consistent offshore trend during time-dependent and advective phases in all three experiments. This suggests that, overall, a canyon serves to intensify downward and offshore velocities, reinforcing the downwelling process.

The results of our experiments are linked to the influence of the canyon on the incoming flow. This implies that a good resolution is needed near the bottom to correctly address the impacts of the topography in the boundary layer and the overall flow dynamics (Clavel-Henry et al., 2019), as well as to avoid numerical errors in the vertical velocities over the steep topography of the canyon (Allen et al., 2003; Dawe and Allen, 2010). Our vertical parameters on sigma coordinates are similar to those of previous studies of flow over topography using ROMS (Rennie et al., 2009; Clavel-Henry et al., 2019; Vergara et al., 2024), which aim to have an increased resolution on the surface and bottom layers. Nonetheless, a sensitivity study is necessary to address the impacts of the vertical resolution and the vertical mixing scheme used, which was out of the scope of this study.

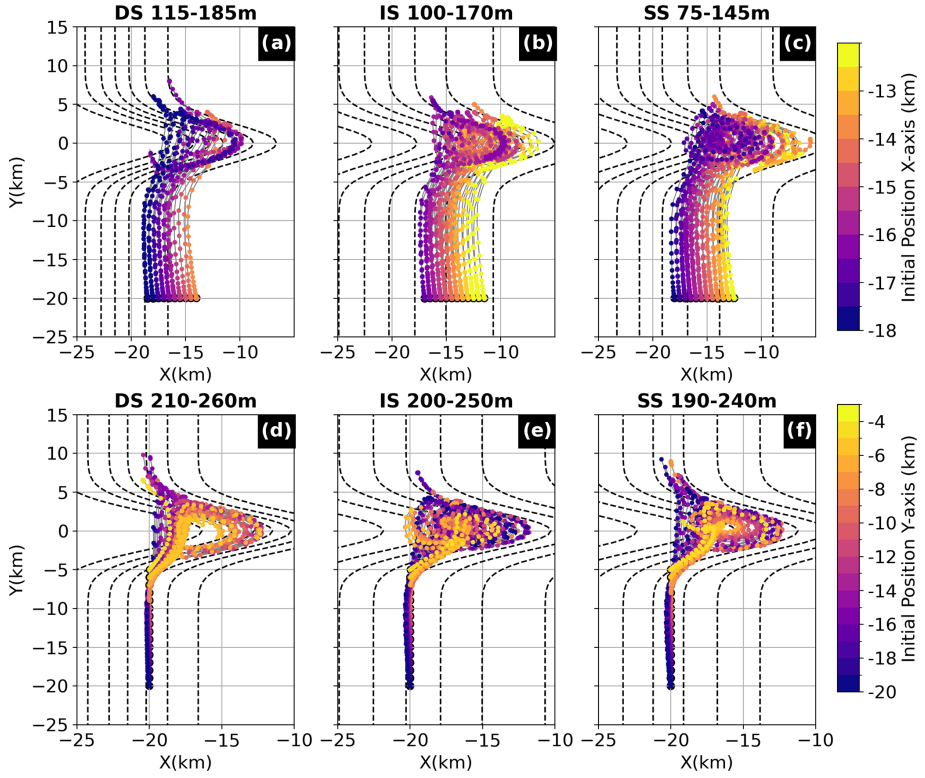

Figure 10. Particles trapped by the canyon (as in Fig. 9) color-coded by their initial position. The colors indicate the initial cross-shore position along the zonal transect at $y = -20$ km **(a–c)** and the initial alongshore position along the meridional transect at $x = -20$ km **(d–f)**.

Dawe and Allen (2010) show that the errors related to the model's resolution could impact how accurately the flow detaches from the canyon walls. Additionally, Ramos-Musalem and Allen (2019) showed that enhanced vertical mixing in a canyon results in a larger upwelling of tracers. Future work should address the impacts of the vertical resolution and mixing profiles on the circulation patterns and particle trajectories.

Previous studies examining downwelling conditions in idealized settings predominantly utilized different approaches to force the circulation, including body-force forcing to simulate remote wind forcing scenarios (Klinck, 1996), local surface wind forcing (Spurgin and Allen, 2014), and combinations of wind forcing and body-force forcing (She and Klinck, 2000; Spurgin and Allen, 2014). In contrast, this study introduces a novel contribution by focusing on a purely wind-forced circulation approach, which is the typical situation of eastern boundary margins during winter. We observe local modifications in surface onshore and bottom offshore transport influenced by the presence of a submarine canyon. Specifically, the onshore velocities observed on the upstream side of the canyon disrupt the bottom Ekman layer, a pattern particularly evident in both the deep and the shallow experiments. These cross-shore velocities are visible during the early stages of the experiments due to canyon-induced effects (as seen in the deep-shelf experiment for day 25) and later during more developed conditions, linked to instabilities interacting with the submarine canyon and the canyon effect (as seen in the intermediate and shallow experiments).

Similarly, offshore velocities on the downstream side can extend to the surface Ekman layer near the coast. The canyon generates onshore velocities beneath the Ekman layer in the upstream region and offshore velocities extending from the bottom Ekman layer up to the base of the surface Ekman layer in the downstream region across all three configurations. The enhancement of offshore velocities on the downstream side may explain the observation of less dense water in that area. Furthermore, the accelerated offshore transport causes the advection of surface water to occur more rapidly compared to scenarios without a canyon.

Three types of continental shelf slopes were examined, with the final 5 d of our experiments facilitating the development of instabilities. Previous studies have primarily focused on the impact of changes in continental shelf slopes on submarine canyons under upwelling conditions, utilizing scaling analyses (Howatt and Allen, 2013) and idealized numerical simulations (Saldías and Allen, 2020). Studies addressing frontal instabilities over a submarine canyon have similarly concentrated on upwelling conditions (Saldías and Allen, 2020). These investigations have demonstrated that steeper slopes and increased stratification lead to a shallower depth of upwelled water and reduced upwelling flux, with

the velocity of incoming flows exhibiting the opposite trend (Howatt and Allen, 2013). Shallower continental shelves result in a more pronounced upwelling surface signal of denser water, albeit with reduced cross-shore transport and faster evolution compared to less inclined configurations (Saldías and Allen, 2020).

In our experiments, the shallow-shelf configuration led to a swift establishment of the downwelling front and increased offshore transport, and it showed greater susceptibility to instabilities than the deep-shelf experiment. The deeper configurations required more time for downwelling waters to form the front. Downwelling circulation resulted in a low Burger number and reduced stratification. Unlike upwelling scenarios, the shelf slope promoted downwelling flux in downwelling conditions, facilitating reduced stratification and vertical movements without significantly affecting net vertical transport. Shallower configurations induced instabilities further offshore, while the canyon modified the instability characteristics, causing density variations. Density anomalies varied mainly in the downstream region, likely associated with changes in instability characteristics passing through the canyon. Studies addressing the stability of the downwelling front have shown that frontal instabilities can grow into large eddies in later well-developed stages (Feliks and Ghil, 1993). Our experiments did not reach that case, which could result from relatively mild wind stress forcing. In the opposite wind case (upwelling favorable), instabilities alter the upwelling front's structure and enhance horizontal variability (Durski and Allen, 2005). Consequently, increased alongshore variability in currents, frontal instabilities, and particle trajectories is expected in the presence of realistic bottom topographies.

The angle between the canyon and the incoming flow influences the pattern of upwelling and downwelling around a submarine canyon. Ahumada-Sempoal et al. (2015) observed a non-traditional pattern in Blanes Canyon, with offshore (onshore) transport upstream (downstream), attributed to the angle between the canyon and the dominant flow field. Their intersection further influences the interaction between the current and the canyon, showing larger velocities when intersecting near the canyon head compared to near the mouth (Alvarez et al., 1996; Jordi et al., 2005). In our simulations, driven solely by wind forcing, the position of the downwelling front and jet depends on wind magnitude and shelf slope. Responses were quicker in the shallow-shelf configuration and slower in the deep-shelf scenario. Observations of the downwelling front off Oregon showed that the front can move around 50 km offshore (Austin and Barth, 2002), farther offshore than the downwelling front in our experiments. This is consistent with having relatively mild wind stress compared with downwelling-favorable winds during realistic winter storms. Moreover, short-term fluctuations, influenced by river discharges, can lead to varied downwelling responses in submarine canyons (Alvarez et al., 1996).

Differences in upwelling and downwelling responses between the upper shelf and within a canyon have been observed in Mackenzie Canyon due to regional wind stress curl conditions (Lin et al., 2021). For instance, wind stress curl can induce upwelling within the canyon even under downwelling-favorable winds, a dynamic not explored here. Furthermore, previous conditions on the adjacent shelf can alter and amplify downwelling responses if they follow wind-driven upwelling events, impacting the density structures advected into the canyon (Wang et al., 2022). Future experiments should consider various jet orientations, wind patterns, and density shelf conditions to comprehensively understand the impact of each component on upwelling and downwelling dynamics around submarine canyons in more realistic settings.

Considering the impact of a submarine canyon on local circulation in a wind-driven downwelling regime, this local circulation could play a crucial role in the biogeochemical conditions along the coast. While the overall contributions favor offshore and downward movement, the local velocities influenced by the canyon could potentially reduce, trap, and even export particles onshore, even under downwelling conditions. Our particle experiments indicated that some particles can become trapped inside the canyon and transported up to 8 km onshore. This phenomenon is more likely to occur with particles initially located inside the canyon or near its mouth, below the shelf-break depth. In such cases, particles may be trapped by the anticyclonic circulation and linger within the canyon for the 15 d of the tracking experiment. For particles carried by the downwelling jet, some can be advected into the canyon and also entrapped by the anticyclonic circulation, a tendency that is more pronounced in the shallow-shelf experiment, which is the case with the largest percentage of particles trapped at the end of the simulation. The trapping effect primarily arises from cross-shore velocities induced by the canyon, primarily observed beneath shelf-break depth. Vertical velocities induced by the canyon do not lead to particle entrapment, primarily due to their smaller magnitudes than those of the horizontal components.

While observations by Ahumada-Sempoal et al. (2015) around the head of the Blanes Canyon have shown similar trapping mechanisms, the process is closely linked to the position of the jet relative to the canyon. This study suggests that our findings offer significant insight into particle trapping in canyons within eastern boundary systems, regions where downwelling conditions are predominantly wind driven rather than influenced by a consistent right-bounded current. Coupled with the alternating favorable winds for upwelling and downwelling commonly observed in these systems, particles trapped during storm events in canyons could be transported further over the shelf by upwelling-favorable winds (Saldías and Allen, 2020). Moreover, submarine canyons experiencing downwelling conditions have been associated with high productivity (Skliris and Djenidi, 2006; Flexas et al., 2008). This productivity has been linked

to whales' preference for using submarine canyons as habitats (Moors-Murphy, 2014). Future observational studies need to focus on how the predicted particle trapping in submarine canyons aligns with actual observations to validate the real impacts of downwelling in the coastal ocean.

5 Conclusions

A series of process-oriented modeling experiments using three distinct bathymetric configurations driven by uniform downwelling-favorable winds revealed that, without a submarine canyon, a downwelling front is formed, leading to frontal instabilities. The introduction of a submarine canyon altered the downwelling circulation, producing pronounced cross-shore velocities near the canyon with asymmetrical patterns of onshore–offshore and downward–upward velocities on the upstream–downstream sides, which is coherent with previous studies of downwelling flows over submarine canyons.

The presence of a submarine canyon can also influence the propagation of frontal instabilities, primarily in the downstream direction. Strong cross-shore velocities induced by the canyon extend to the surface and interact with the surface Ekman layer. Moreover, while the net effect of the canyon is to enhance downwelling, local onshore velocities in the vicinity of the canyon lead to an anticyclonic circulation inside the canyon that can trap particles for the entire simulation period (15 d). This particle-trapping phenomenon could affect both particles traveling along the continental slope with the incoming current and those initially located inside or over the canyon at the onset of the downwelling event. These results highlight the potentially pivotal role of submarine canyons in counteracting the effects of downwelling regimes by opposing the offshore bottom Ekman transport in the contiguous continental shelf. Future studies should investigate the implications of this mechanism and consider more realistic wind forcing scenarios to enhance our understanding of the complex interactions between submarine canyons and downwelling conditions.

Data availability. Data are available upon request to the main author.

Author contributions. GS and SA generated the idea to be studied; PF undertook all the final analyses and wrote the original version of the manuscript. GS and SA reviewed and corrected the draft version.

Competing interests. The contact author has declared that none of the authors has any competing interests.

Disclaimer. Publisher's note: Copernicus Publications remains neutral with regard to jurisdictional claims made in the text, published maps, institutional affiliations, or any other geographical representation in this paper. While Copernicus Publications makes every effort to include appropriate place names, the final responsibility lies with the authors.

Special issue statement. This article is part of the special issue "Oceanography at coastal scales: modelling, coupling, observations, and applications". It is not associated with a conference.

Acknowledgements. Susan E. Allen has been partially funded by NSERC Discovery (RGPIN-2022-03112). We also thank Compute Canada RAC 2022 (grant number RRG 1792) and the Digital Research Alliance of Canada RAC 2023 (grant number RRG 4603). Gonzalo S. Saldías was partially funded by FONDECYT (1220167) and the COPAS Coastal ANID project (FB210021). This research was partially supported by the supercomputing infrastructure of the NLHPC (Powered@NLHPC, CCSS210001).

Financial support. This research has been supported by the Fondo Nacional de Desarrollo Científico y Tecnológico (grant no. 1220167).

Review statement. This paper was edited by Davide Bonaldo and reviewed by Miguel-Angel Ahumada-Sempoal, Jochen Kämpf, and one anonymous referee.

References

Ahumada-Sempoal, M.-A., Flexas, M. d. M., Bernardello, R., Bahamon, N., Cruzado, A., and Reyes-Hernández, C.: Shelf-slope exchanges and particle dispersion in Blanes submarine canyon (NW Mediterranean Sea): A numerical study, Cont. Shelf Res., 109, 35–45, 2015.

Allen, S., Vindeirinho, C., Thomson, R., Foreman, M. G., and Mackas, D.: Physical and biological processes over a submarine canyon during an upwelling event, Can. J. Fish. Aquat. Sci., 58, 671–684, 2001.

Allen, S., Dinniman, M., Klinck, J., Gorby, D., Hewett, A., and Hickey, B.: On vertical advection truncation errors in terrain-following numerical models: Comparison to a laboratory model for upwelling over submarine canyons, J. Geophys. Res., 108, 3003, https://doi.org/10.1029/2001JC000978, 2003.

Allen, S. E. and Durrieu de Madron, X.: A review of the role of submarine canyons in deep-ocean exchange with the shelf, Ocean Sci., 5, 607–620, https://doi.org/10.5194/os-5-607-2009, 2009.

Allen, S. E. and Hickey, B. M.: Dynamics of advection-driven upwelling over a shelf break submarine canyon, J. Geophys. Res.-Oceans, 115, C08018, https://doi.org/10.1029/2009JC005731, 2010.

Alvarez, A., Tintoré, J., and Sabatés, A.: Flow modification and shelf-slope exchange induced by a submarine canyon off the

northeast Spanish coast, J. Geophys. Res.-Oceans, 101, 12043–12055, 1996.

Austin, J. A. and Barth, J. A.: Drifter behavior on the Oregon–Washington shelf during downwelling-favorable winds, J. Phys. Oceanogr., 32, 3132–3144, 2002.

Austin, J. A. and Lentz, S. J.: The inner shelf response to wind-driven upwelling and downwelling, J. Phys. Oceanogr., 32, 2171–2193, 2002.

Brink, K.: Continental shelf baroclinic instability. Part I: Relaxation from upwelling or downwelling, J. Phys. Oceanogr., 46, 551–568, 2016.

Brink, K.: The effect of alongshore wind stress on a buoyancy current's stability, Cont. Shelf Res., 272, 105149, https://doi.org/10.1016/j.csr.2023.105149, 2024.

Brun, L., Pairaud, I., Jacinto, R. S., Garreau, P., and Dennielou, B.: Strong hydrodynamic processes observed in the Mediterranean Cassidaigne submarine canyon, Front. Mar. Sci., 10, 1078831, https://doi.org/10.3389/fmars.2023.1078831, 2023.

Castelao, R. M. and Barth, J. A.: The relative importance of wind strength and along-shelf bathymetric variations on the separation of a coastal upwelling jet, J. Phys. Oceanogr., 36, 412–425, 2006.

Ceramicola, S., Amaro, T., Amblas, D., Cagatay, N., Carniel, S., Chiocci, F. L., and Briand, F.: Submarine canyon dynamics–executive summary, in: CIESM monograph 47 submarine canyon dynamics in the Mediterranean and tributary seas – An integrated geological, oceanographic and biological perspective, edited by: Briand, F., CIESM Publisher, p. 232, https://ciesm.org/online/monographs/full/CIESM_Workshop_Monograph_47.pdf (last access: 12 March 2025), 2015.

Chapman, D. C.: Numerical treatment of cross-shelf open boundaries in a barotropic coastal ocean model, J. Phys. Oceanogr., 15, 1060–1075, 1985.

Clavel-Henry, M., Solé, J., Ahumada-Sempoal, M.-Á., Bahamon, N., Briton, F., Rotllant, G., and Company, J. B.: Influence of the summer deep-sea circulations on passive drifts among the submarine canyons in the northwestern Mediterranean Sea, Ocean Sci., 15, 1745–1759, https://doi.org/10.5194/os-15-1745-2019, 2019.

Connolly, T. P. and Hickey, B. M.: Regional impact of submarine canyons during seasonal upwelling, J. Geophys. Res.-Oceans, 119, 953–975, 2014.

Dawe, J. T. and Allen, S. E.: Solution convergence of flow over steep topography in a numerical model of canyon upwelling, J. Geophys. Res.-Oceans, 115, C05008, https://doi.org/10.1029/2009JC005597, 2010.

Delandmeter, P. and van Sebille, E.: The Parcels v2.0 Lagrangian framework: new field interpolation schemes, Geosci. Model Dev., 12, 3571–3584, https://doi.org/10.5194/gmd-12-3571-2019, 2019.

De Leo, F. C., Smith, C. R., Rowden, A. A., Bowden, D. A., and Clark, M. R.: Submarine canyons: hotspots of benthic biomass and productivity in the deep sea, P. Roy. Soc. B, 277, 2783–2792, 2010.

Dinniman, M. S. and Klinck, J. M.: The influence of open versus periodic alongshore boundaries on circulation near submarine canyons, J. Atmos. Ocean. Tech., 19, 1722–1737, 2002.

Durski, S. M. and Allen, J.: Finite-amplitude evolution of instabilities associated with the coastal upwelling front, J. Phys. Oceanogr., 35, 1606–1628, 2005.

Feliks, Y. and Ghil, M.: Downwelling-front instability and eddy formation in the Eastern Mediterranean, J. Phys. Oceanogr., 23, 61–78, 1993.

Flather, R.: A tidal model of the northwest European continental shelf, Mem. Soc. Roy. Sci. Liege, 10, 141–164, 1976.

Flexas, M. d. M., Boyer, D., Espino, M., Puigdefàbregas, J., Rubio, A., and Company, J.: Circulation over a submarine canyon in the NW Mediterranean, J. Geophys. Res.-Oceans, 113, C12002, https://doi.org/10.1029/2006JC003998, 2008.

Gan, J. and Allen, J. S.: On open boundary conditions for a limited-area coastal model off Oregon. Part 1: Response to idealized wind forcing, Ocean Model., 8, 115–133, 2005.

Hickey, B. M.: The response of a steep-sided, narrow canyon to time-variable wind forcing, J. Phys. Oceanogr., 27, 697–726, 1997.

Howatt, T. and Allen, S.: Impact of the continental shelf slope on upwelling through submarine canyons, J. Geophys. Res.-Oceans, 118, 5814–5828, 2013.

Jordi, A., Orfila, A., Basterretxea, G., and Tintoré, J.: Shelf-slope exchanges by frontal variability in a steep submarine canyon, Prog. Oceanogr., 66, 120–141, 2005.

Kämpf, J.: Transient wind-driven upwelling in a submarine canyon: A process-oriented modeling study, J. Geophys. Res.-Oceans, 111, C11011, https://doi.org/10.1029/2006JC003497, 2006.

Kämpf, J.: On the magnitude of upwelling fluxes in shelf-break canyons, Cont. Shelf Res., 27, 2211–2223, 2007.

Kämpf, J.: On the interaction of time-variable flows with a shelf-break canyon, J. Phys. Oceanogr., 39, 248–260, 2009.

Kämpf, J.: Lee effects of localized upwelling in a shelf-break canyon, Cont. Shelf Res., 42, 78–88, 2012.

Kämpf, J.: On the dynamics of canyon–flow interactions, J. Mar. Sci. Eng., 6, 129, https://doi.org/10.3390/jmse6040129, 2018.

Kämpf, J.: Extreme bed shear stress during coastal downwelling, Ocean Dynam., 69, 581–597, 2019.

Klinck, J. M.: Circulation near submarine canyons: A modeling study, J. Geophys. Res.-Oceans, 101, 1211–1223, 1996.

Lentz, S. J. and Fewings, M. R.: The wind-and wave-driven inner-shelf circulation, Annu. Rev. Mar. Sci., 4, 317–343, 2012.

Li, X., Zhang, W., and Rong, Z.: The Interaction Between Warm-Core Rings and Submarine Canyons and Its Influence on the Onshore Transport of Offshore Waters, J. Geophys. Res.-Oceans, 126, e2021JC017989, https://doi.org/10.1029/2021JC017989, 2021.

Lin, P., Pickart, R. S., Fissel, D. B., Borg, K., Melling, H., and Wiese, F. K.: On the nature of wind-forced upwelling and downwelling in Mackenzie Canyon, Beaufort Sea, Prog. Oceanogr., 198, 102674, https://doi.org/10.1016/j.pocean.2021.102674, 2021.

Mellor, G. L. and Yamada, T.: Development of a turbulence closure model for geophysical fluid problems, Rev. Geophys., 20, 851–875, 1982.

Moors-Murphy, H. B.: Submarine canyons as important habitat for cetaceans, with special reference to the Gully: a review, Deep-Sea Res. Pt. II, 104, 6–19, 2014.

Mordy, C. W., Stabeno, P. J., Kachel, N. B., Kachel, D., Ladd, C., Zimmermann, M., Hermann, A. J., Coyle, K. O., and Doyle,

M. J.: Patterns of flow in the canyons of the northern Gulf of Alaska, Deep-Sea Res. Part II, 165, 203–220, 2019.

Orlanski, I.: A simple boundary condition for unbounded hyperbolic flows, J. Comput. Phys., 21, 251–269, 1976.

Ramos-Musalem, K. and Allen, S. E.: The impact of locally enhanced vertical diffusivity on the cross-shelf transport of tracers induced by a submarine canyon, J. Phys. Oceanogr., 49, 561–584, 2019.

Rennie, S. J., Pattiaratchi, C. B., and McCauley, R. D.: Numerical simulation of the circulation within the Perth Submarine Canyon, Western Australia, Cont. Shelf Res., 29, 2020–2036, 2009.

Saldías, G. S. and Allen, S. E.: The influence of a submarine canyon on the circulation and cross-shore exchanges around an upwelling front, J. Phys. Oceanogr., 50, 1677–1698, 2020.

Santora, J. A., Zeno, R., Dorman, J. G., and Sydeman, W. J.: Submarine canyons represent an essential habitat network for krill hotspots in a Large Marine Ecosystem, Sci. Rep., 8, 7579, https://doi.org/10.1038/s41598-018-25742-9, 2018.

Shchepetkin, A. F. and McWilliams, J. C.: A method for computing horizontal pressure-gradient force in an oceanic model with a nonaligned vertical coordinate, J. Geophys. Res., 108, 3090, https://doi.org/10.1029/2001JC001047, 2003.

Shchepetkin, A. F. and McWilliams, J. C.: The regional oceanic modeling system (ROMS): a split-explicit, free-surface, topography-following-coordinate oceanic model, Ocean Model., 9, 347–404, 2005.

Shchepetkin, A. F. and McWilliams, J. C.: Correction and commentary for "Ocean forecasting in terrain-following coordinates: Formulation and skill assessment of the regional ocean modeling system" by Haidvogel et al., J. Comp. Phys. 227, pp. 3595–3624, J. Comput. Phys., 228, 8985–9000, 2009.

She, J. and Klinck, J. M.: Flow near submarine canyons driven by constant winds, J. Geophys. Res.-Oceans, 105, 28671–28694, 2000.

Skliris, N. and Djenidi, S.: Plankton dynamics controlled by hydrodynamic processes near a submarine canyon off NW corsican coast: a numerical modelling study, Cont. Shelf Res., 26, 1336–1358, 2006.

Skliris, N., Goffart, A., Hecq, J.-H., and Djenidi, S.: Shelf-slope exchanges associated with a steep submarine canyon off Calvi (Corsica, NW Mediterranean Sea): A modeling approach, J. Geophys. Res.-Oceans, 106, 19883–19901, 2001.

Skliris, N., Hecq, J.-H., and Djenidi, S.: Water fluxes at an ocean margin in the presence of a submarine canyon, J. Mar. Syst., 32, 239–251, 2002.

Sobarzo, M., Saldías, G. S., Tapia, F. J., Bravo, L., Moffat, C., and Largier, J. L.: On subsurface cooling associated with the Biobio River Canyon (Chile), J. Geophys. Res.-Oceans, 121, 4568–4584, 2016.

Song, Y. and Haidvogel, D.: A semi-implicit ocean circulation model using a generalized topography-following coordinate system, J. Comput. Phys., 115, 228–244, 1994.

Spurgin, J. M. and Allen, S. E.: Flow dynamics around downwelling submarine canyons, Ocean Sci., 10, 799–819, https://doi.org/10.5194/os-10-799-2014, 2014.

Vergara, O. A., Figueroa, P. A., Salas, C., Vásquez, S. I., Muñoz, R., and Saldías, G. S.: The influence of the Biobio Canyon on the circulation and coastal upwelling/downwelling off central Chile, Cont. Shelf Res., 282, 105335, https://doi.org/10.1016/j.csr.2024.105335, 2024.

Wang, H., Gong, D., Friedrichs, M. A., Harris, C. K., Miles, T., Yu, H.-C., and Zhang, Y.: A Cycle of Wind-Driven Canyon Upwelling and Downwelling at Wilmington Canyon and the Evolution of Canyon-Upwelled Dense Water on the MAB Shelf, Front. Mar. Sci., 9, 866075, https://doi.org/10.3389/fmars.2022.866075, 2022.

Whitney, M. M. and Allen, J.: Coastal wind-driven circulation in the vicinity of a bank. Part I: Modeling flow over idealized symmetric banks, J. Phys. Oceanogr., 39, 1273–1297, 2009.

Zhang, T. and Yankovsky, A. E.: On the nature of cross-isobath energy fluxes in topographically modified barotropic semidiurnal Kelvin waves, J. Geophys. Res.-Oceans, 121, 3058–3074, 2016.

Zhang, W. and Lentz, S. J.: Wind-driven circulation in a shelf valley. Part I: Mechanism of the asymmetrical response to along-shelf winds in opposite directions, J. Phys. Oceanogr., 47, 2927–2947, 2017.